Polymer 102 (2016) 73–83

Contents lists available at ScienceDirect

Polymer

journal homepage: www.elsevier.com/locate/polymer

Lightweight micro-cellular plastics from polylactide/polyolefin hybrids

Yuewen Xu [a], Paula Delgado [a], Alexander D. Todd [a], Jesse Loi [b], Stacey A. Saba [b], Ryan J. McEneany [c], Ted Tower [c], Vasily Topolkaraev [c, *], Christopher W. Macosko [b, *], Marc A. Hillmyer [a, *]

[a] Department of Chemistry, University of Minnesota, Minneapolis, MN 55455, USA
[b] Department of Chemical Engineering and Materials Science, University of Minnesota, Minneapolis, MN 55455, USA
[c] Corporate Research & Engineering, Kimberly-Clark Corporation, Neenah, WI 54957, USA

ARTICLE INFO

Article history:
Received 8 July 2016
Received in revised form
22 August 2016
Accepted 28 August 2016
Available online 30 August 2016

Keywords:
Polylactide
Polymer blend
Lightweight polymer

ABSTRACT

Semi-crystalline polylactide (PLA)/polyolefin multi-component blends were used as precursors for the generation of a new class of micro-cellular polymers. Either a polypropylene-based elastomer (PBE) or polypropylene (PP) homopolymer were utilized as dispersed phases at the 10 wt% level. An epoxy-functionalized terpolymer (PEGMMA) was introduced (1 wt%) as a reactive compatibilizer to reduce the dispersed phase droplet size and provide sufficient adhesion between the matrix and dispersed phase. In addition, a polyalkylene glycol liquid (PAG) was added to the blend (4 wt%) to serve as a PLA plasticizer and interfacial modifier. The multicomponent blends exhibited significant increases in strain at break as compared to neat PLA and were subjected to a range of uniaxial strains (10–90%) at room temperature. These cold drawn materials exhibited nearly constant cross-sectional area and fine micro-cellular structures, as revealed by scanning electron microscopy. Distinct different voiding mechanisms observed for the PBE- and PP-containing blends were ascribed to the differences in the dispersed phase elastic moduli and deformability. The material density of cold drawn blends was reduced by up to 34% when compared to the precursor blends without a noticeable change in cross-sectional area. The novel low-density microcellular PLA blends demonstrated outstanding mechanical properties such as high strength, high modulus, substantial ductility, and a 14-fold increase in impact resistance as compared to PLA homopolymer.

1. Introduction

Polylactide (PLA) is a biodegradable, biorenewable and biocompatible thermoplastic aliphatic polyester used in commercial products [1–7]. Despite PLA's commercial presence, its widespread implementation has been hampered by poor melt strength, slow crystallization kinetics, and brittleness. Moreover, the high density of PLA compared with conventional polyolefins increases product costs [8,9]. Therefore, methodologies that improve its toughness, processability and to lower its density are of considerable commercial interest. One strategy to lower the density of PLA is to incorporate cells or voids dispersed throughout the material. Such cellular plastics or foams can be obtained by a variety of methods [10]. For example, cold-stretching has been used to produce micro-cellular materials in semicrystalline polymers such as polyethylene (PE) [11,12], polypropylene (PP) [13,14], and polytetrafluoroethylene (PTFE) [15,16]. The pores/voids are obtained by uniaxially stretching an ordered crystalline polymer at room temperature (cold-drawing), and interconnected voids form in response to the loading. In another example, PLA-based foams have been fabricated using foam injection molding to achieve void contents as high as 65% [17–20].

The formation of cavities/voids in a number of semi-crystalline polymers by cavitation can take place when the polymer is stretched uni- or bi-axially. Numerous studies have been conducted to investigate cavitation in semi-crystalline polymers, where a three dimensional local state of stress is typically necessary for initiation [21,22]. The cavities in semi-crystalline polymers can

* Corresponding authors.
E-mail addresses: vasiltop@kcc.com (V. Topolkaraev), macosko@umn.edu (C.W. Macosko), hillmyer@umn.edu (M.A. Hillmyer).

http://dx.doi.org/10.1016/j.polymer.2016.08.102
0032-3861/

form inside amorphous phase between lamella when the tensile strength of amorphous phase is lower than the yield stress associated with plastic deformation of the crystalline phase [23]. However, the voiding mechanism in polymer composites and blends, where debonding between matrix and inclusions takes place before or around the yield point has been less studied [24]. More importantly, these mechanisms have not been linked to the opportunity of developing nano-cellular materials with enhanced performance.

In pursuit of ductile, low density PLA with a high void content and small pore sizes, we investigated a series of PLA/polyolefin multi-component blends. After uniaxially stretching, SEM imaging of the cross-sections revealed the presence of closed-cell pores. Furthermore, negligible necking was observed during cold-drawing of precursor blends as the cross-sectional area remained nearly constant suggesting dilational growth of micro-voids, which corresponds to the expansion or enlargement of voids during drawing [23,25,26]. Polypropylene (PP) or a polypropylene-based elastomer (PBE) were incorporated at 10 wt% as toughness and ductility modifying additives and an epoxy-functional terpolymer (PEGMMA) was used as a reactive compatibilizer (1 wt%) as described in our previous work [27]. In the present case, a polyalkylene glycol liquid (PAG) was added at low levels to serve as a PLA plasticizer and interfacial modifier to facilitate void formation. The cavities of PLA multi-component blends studied in this system are primarily the result of debonding between PLA matrix and polyolefin dispersed phase under uniaxial extension. Nanometer scale cavities, ostensibly from cavitation of the PLA matrix, also appear to contribute to the overall cellular structure [28]. In this work, we explore the fundamental aspects of micro-void initiation and growth in multicomponent PLA/polyolefin blends to enable development of new PLA based low-density materials with excellent mechanical properties.

2. Results and discussion

2.1. Polymer blend preparation

Polymer blends were fabricated using a co-rotating twin-screw extruder unless otherwise noted. The matrix (PLA), dispersed phase (PBE or PP) and reactive compatibilizer (PEGMMA) were manually premixed in the appropriate mass ratio prior to introduction into the extruder. When included, PAG was added in the third zone of the extruder via liquid injection. All polymer blends were subsequently pelletized prior to further processing and analysis. For additional details, please see the supporting information.

2.2. Blend morphology and glass transition temperature

The morphology of blends prior to cold-drawing was initially investigated by SEM to identify the roles of the polymer additives in the PLA matrix. The blends were either cryo-fractured at the cross-section of the dog-bone specimen or cryo-microtomed prior to SEM analysis. Fig. 1 presents the SEM micrographs of a PLA/PBE binary blend, ternary blends with PEGMMA or PAG, and quaternary blends containing both PEGMMA and PAG. The PLA/PBE (90/10) binary blend has large PBE droplets with d_n (number average particle diameter) = 6.2 μm ± 1.3 μm (Fig. 1a and b). Consistent with our previous results, the addition of 1 wt% PEGMMA significantly reduces d_n to 1.5 μm ± 0.1 μm (Fig. 1c and d) [29,30]. In ternary blends containing 4 wt% PAG there is no significant reduction in PBE particle size (d_n = 6.1 ± 0.6 μm) compared with the binary blend (Fig. 1e and f); unlike PEGMMA, PAG does not behave as a compatibilizer in these blends. Small (200–500 nm) droplets scattered throughout PLA matrix were assigned to PAG on the basis of our analysis of PAG/PLA binary blends (Fig. S2 in Supporting Information). This result supports lack of miscibility between PAG and PLA. There is no evidence for incorporation of the PAG by the dispersed PBE phase from Fig. 1e and f [31,32]. Moreover, the cryo-microtomed sample of PLA/PBE/PAG (90/10/4) blend (Fig. 1f) illustrates the poor adhesion between the PBE and PLA. Phase separated PAG was also found in the PLA/PBE/PEGMMA/PAG quaternary blends (Fig. 1g and h). These blends contained small PBE droplets (d_n = 2.0 ± 0.2 μm) suggesting that the inclusion of PAG did not significantly interfere with the compatibilizing ability of PEGMMA. Interestingly, comparing cryo-microtomed images 1d and 1h, the PBE droplets appeared to lodge from the blends containing PAG. ^{1}H NMR spectroscopy was used to analyze PAG (see Fig. S1) and we determined that the polymer consisted primarily of propylene oxide repeat units thus rendering it less compatible with PLA as compared to polyethylene glycol (PEG). PEG is known to be miscible with PLA [33,34], whereas the miscibility of polypropylene glycol (PPG) with PLA decreases as the molar mass of PPG increases [35,36]. Thus, it is reasonable that phase separated PAG can migrate to the respective interfaces between the blend components.

The compatibility between the PAG and PLA was assessed by evaluating the glass transition temperature (T_g) of the blends by DSC. Fig. S5 shows that the T_g values for PLA in the PLA/PBE and PLA/PBE/PEGMMA blends were very similar to neat PLA (59 °C). However, upon addition of the PAG to a PLA/PBE binary blend or to PLA/PBE/PEGMMA ternary blends, the T_g of the PLA dropped to approximately 48 °C. This decrease of the T_g in the corresponding blend along with phase separated PAG in the PLA matrix suggests a partial miscibility of PLA and PAG thus leading to plasticization. Replacing the PBE with the more rigid polypropylene (PP) led to similar differences in the T_g of PLA (Fig. S5).

2.3. Tensile testing

To obtain useful cellular polymers via cold drawing, the matrix should be relatively ductile [37,38]. Stress-strain curves for all the PLA/PBE samples are shown in Fig. 2. As we demonstrated previously [27], the inclusion of 1 wt% PEGMMA to the brittle PLA/PBE blend increased the ultimate elongation at break (ε_b) two-fold, while the modulus (E) and the yield stress (σ_{YS}) remained nearly unchanged (Table 1) compared to the corresponding uncompatibilized binary blend. The increase in the elongation at break was attributed to the improved interfacial adhesion and thus stress transfer between the dispersed and matrix phases during ductile deformation [39–43]. The plasticizing and micro-voids initiating effects associated with PAG were apparent upon addition to the uncompatibilized PLA/PBE binary blends. The ε_b values for PLA/PBE/PAG samples increased three-fold (Table 1) as compared to the PLA/PBE binary blends reflecting the enhanced ductility of the PLA matrix. Surprisingly, the σ_{YS} was reduced by approximately 40% in both PLA/PBE/PAG and PLA/PBE/PEGMMA/PAG systems as compared to the corresponding PLA/PBE and PLA/PAG binary blends and close to 3-fold versus neat PLA. Mechanisms of such dramatic reduction in σ_{YS} are posited to be associated with the role of PAG as a plasticizer and debonding/micro-voids growth initiator (vide infra).

The compression-molded samples of the PLA/PBE/PEGMMA/PAG quaternary blends exhibited a 6-fold increase in the elongation at break (ε_b) values compared with neat PLA (Table 1 and Fig. 2). A similar increase was observed in our earlier work [44]. The tensile specimen gauge area after stretching showed homogenously distributed whitening and negligible change (>1% for both thickness and width) in the cross-sectional dimensions as illustrated in Fig. 3. On the whole, these tensile results were almost identical to those obtained with the related PP system (Fig. S4, Table S2).

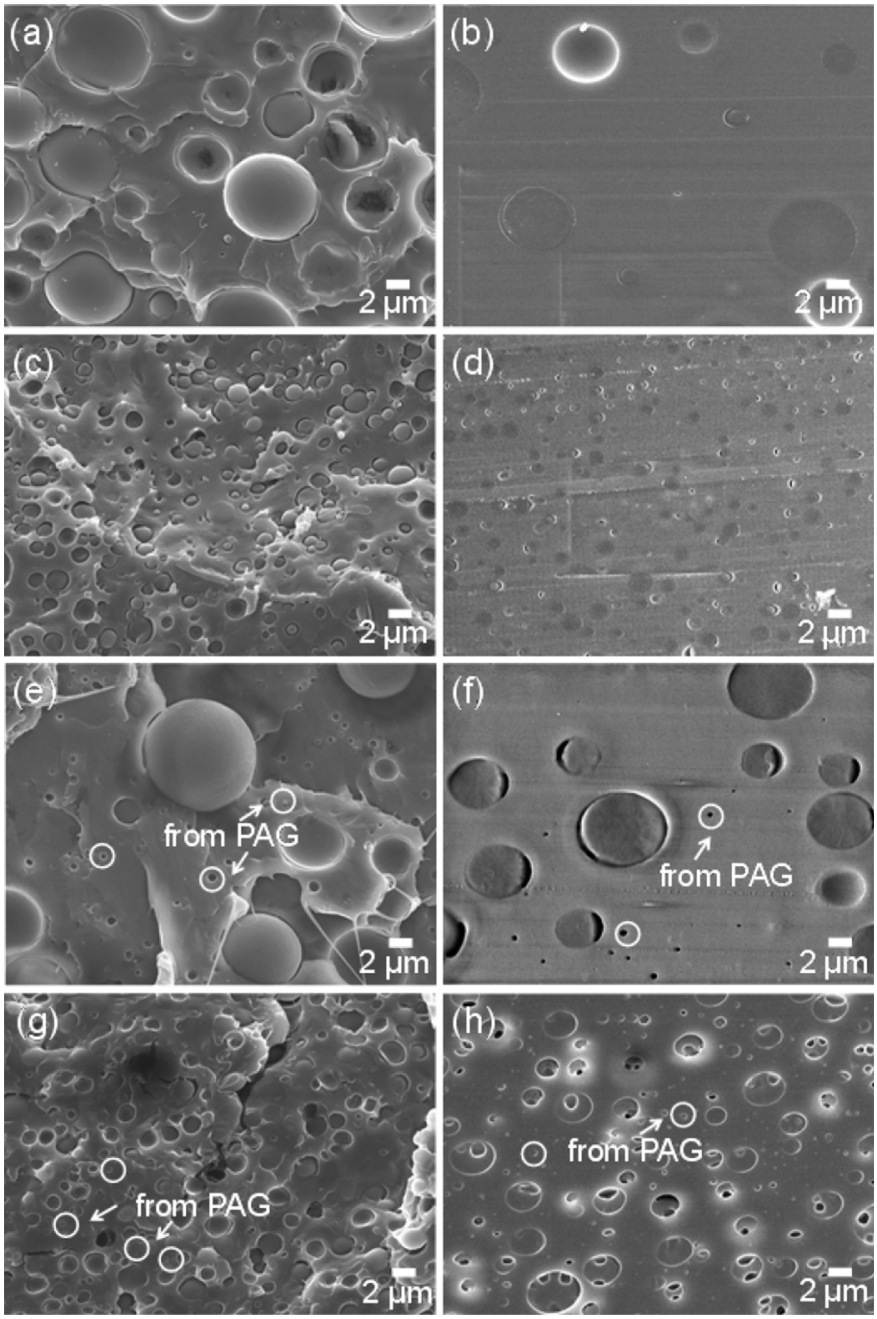

Fig. 1. SEM micrographs, left side cryo-fractured, right cryo-microtomed, of (a,b) PLA/PBE (90/10) (b is from Ref. [27]); (c,d) PLA/PBE/PEGMMA (90/10/1); (e,f) PLA/PBE/PAG (90/10/4); (g,h) PLA/PBE/PEGMMA/PAG (90/10/1/4).

2.4. Structure of cold-drawn samples

To elucidate the structure of multi-component PLA blends after cold-drawing, the dog-bone shaped specimens of both PLA/PBE and PLA/PP binary blends were subjected to cold drawing at different strains (10–90%) prior to failure. To establish a complete profile of the structures formed in the stretched samples, strained specimens were cryo-fractured transverse to the axial strain to expose the xz plane or parallel to the axial strain to expose the yz plane (Fig. 4a). The micrographs on the left column correspond to samples fractured transverse to the axial strain, while those on the right column correspond to the same sample fractured parallel to the axial strain. The SEM micrographs of the PLA/PBE/PEGMMA/PAG (90/10/1/4) blend stretched from 10% to 90% strain (at 20% intervals) are presented in Fig. 4b–k. At 10% strain, the PBE droplets underwent minor deformation, evidenced by the dents/cavities on the droplet surface (Fig. 4c). As the strain was increased (above 30% strain), the PBE droplets elongated along the stretch direction, started to debond, and underwent further deformation. This process leaves gaps (in μm range) at the interface between the matrix PLA and dispersed PBE, which becomes more prominent at higher strains (Fig. 4f–k). A combination of the depressions on the droplet surface and the gaps between the matrix and the dispersed phase comprise the cellular nature of this multi-component blend.

Conversely, for the PLA/PP/PEGMMA/PAG (90/10/1/4) blend, the PP droplets (larger than PBE in size) underwent very low

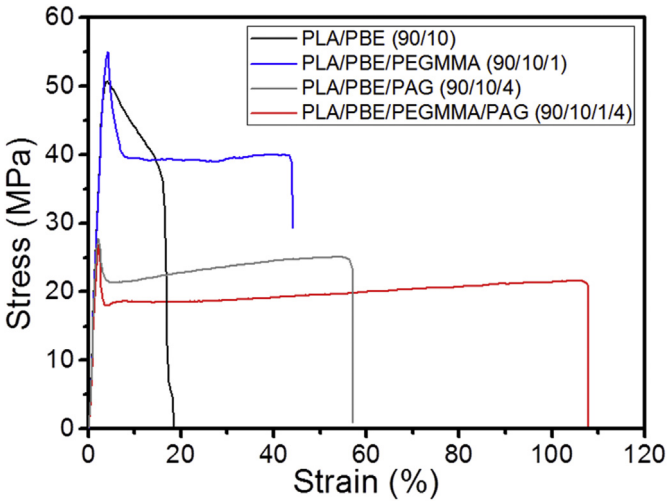

Fig. 2. Representative stress-strain curves of PLA/PBE blends with PEGMMA and/or PAG.

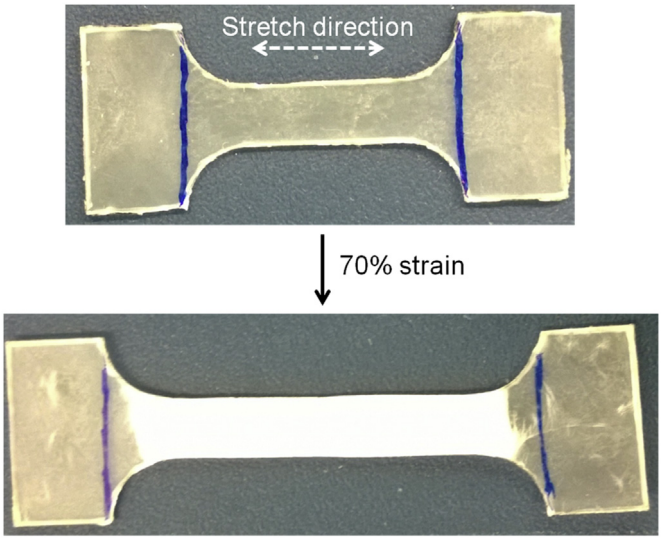

Fig. 3. Photos of the PLA/PBE/PEGMMA/PAG (90/10/1/4) samples before and after uniaxial extension at room temperature. PLA/PP/PEGMMA/PAG (90/10/1/4) displays a similar drawing and whitening effect.

degrees of deformation according to both the transverse and parallel images (represented in the left and right column of Fig. 5, respectively). Even at high strain levels, i.e. 90%, the PP droplets seem to be stretched to only a small extent along the strain direction (Fig. 5j) and show no dents/cavities on particle surface. The contrast in droplet deformation is clear in the PBE droplet at the same strain (Fig. 4j) and can be ascribed to the high elastic modulus of PP as compared to PBE (1000 MPa of PP vs. 14 MPa of PBE). As a consequence, the PLA/PP/PEGMMA/PAG blend responds differently upon stress loading. The debonding mechanism predominates over dispersed phase elongation, leaving cellular characteristics primarily comprised of gaps between PLA and PP. In both cases, the pores generated are not interconnected, and the cellular structure obtained here corresponds to a closed pore structure.

These slightly different mechanisms between the PBE and PP were further confirmed by cryo-microtoming the surface of stretched blends. Two representative images of PLA/PBE/PEGMMA/PAG (90/10/1/4) and PLA/PP/PEGMMA/PAG (90/10/1/4) blends scanned parallel (plane yz) to the stretch direction at a strain of 50% are presented in Fig. 6a and b and Fig. S6. When PBE was used as a dispersed phase (Fig. 6a), the dispersed droplets clearly showed signs of depressions on the surface along with significant deformation in shape, consistent with that observed from the cryo-fractured samples. In comparison, when PP was used as a dispersed phase (Fig. 6b and S7), the droplets showed only minor levels of deformation. A fraction of sub-micrometer and even nanometer scale voids and cavities in spaces between larger polyolefin inclusions are attributed to the cavitation of PLA matrix under uni-axial extension and/or void growth from the phase separated PAG.

Closer inspection of the interface in the high strain (90%) samples reveals nano-fibril linkages between the matrix and dispersed phase. The fibril structure at the interface is typically an indication of imperfect adhesion between phases [40,45,46]. Similar fibril structure has been previously observed by Anderson et al., where a PLA-*b*-PE block polymer was utilized as a compatibilizer in an immiscible PLA/LLDPE blend. The PE and PLA phases displayed significant increase in adhesion strength in the presence of the compatibilizer [46]. Nanoscale fibrils could be identified when either PBE or PP was applied as the dispersed phase, as shown in Fig. 7. This nano-fibril linkage between phases was observed in the majority of particles and existed over nearly all the range of strains screened. We suggest that an intermediate level of adhesion is needed to initiate depressions on droplet surface and gaping at the interface, as well as stabilize the void growth during cold drawing. The adhesion strength between PLA and PP/PBE in the presence of PEGMMA was uncovered in our previous study; a peel strength of 700 ± 250 N/m for PLA/PBE and 2300 ± 350 N/m for PLA/PP was observed [27]. On the other hand, weak adhesion would not render sufficient mechanical integrity as the two phases would easily debond, and thus particle deformation and a stable micro-void growth would not be possible. Support for this hypothesis was demonstrated through mechanical analysis of PLA/PBE/PAG (90/10/

Table 1
Mechanical characteristics of polymer blends used.

Material[a]	Composition[b]	E (GPa)	ε_b (%)	σ_{YS} (MPa)
PLA	100	2.2 ± 0.2	7.6 ± 1	78 ± 6
PP	100	1.0 ± 0.03	28 ± 5	41 ± 5
PBE	100	0.014 ± 0.002	780 ± 80	2.8 ± 0.3
PLA/PBE	90/10	1.6 ± 0.1	18 ± 2	50 ± 3
PLA/PBE/PEGMMA	90/10/1	1.8 ± 0.1	41 ± 6	53 ± 3
PLA/PBE/PAG	90/10/4	1.5 ± 0.2	57 ± 10	30 ± 2
PLA/PBE/PEGMMA/PAG	90/10/1/4	1.7 ± 0.1	110 ± 20	24 ± 2
PLA/PAG	100/4	2.1 ± 0.1	10 ± 2	55 ± 3

[a] Samples aged for 18 h at 25 °C [27].
[b] Composition ratio by mass.

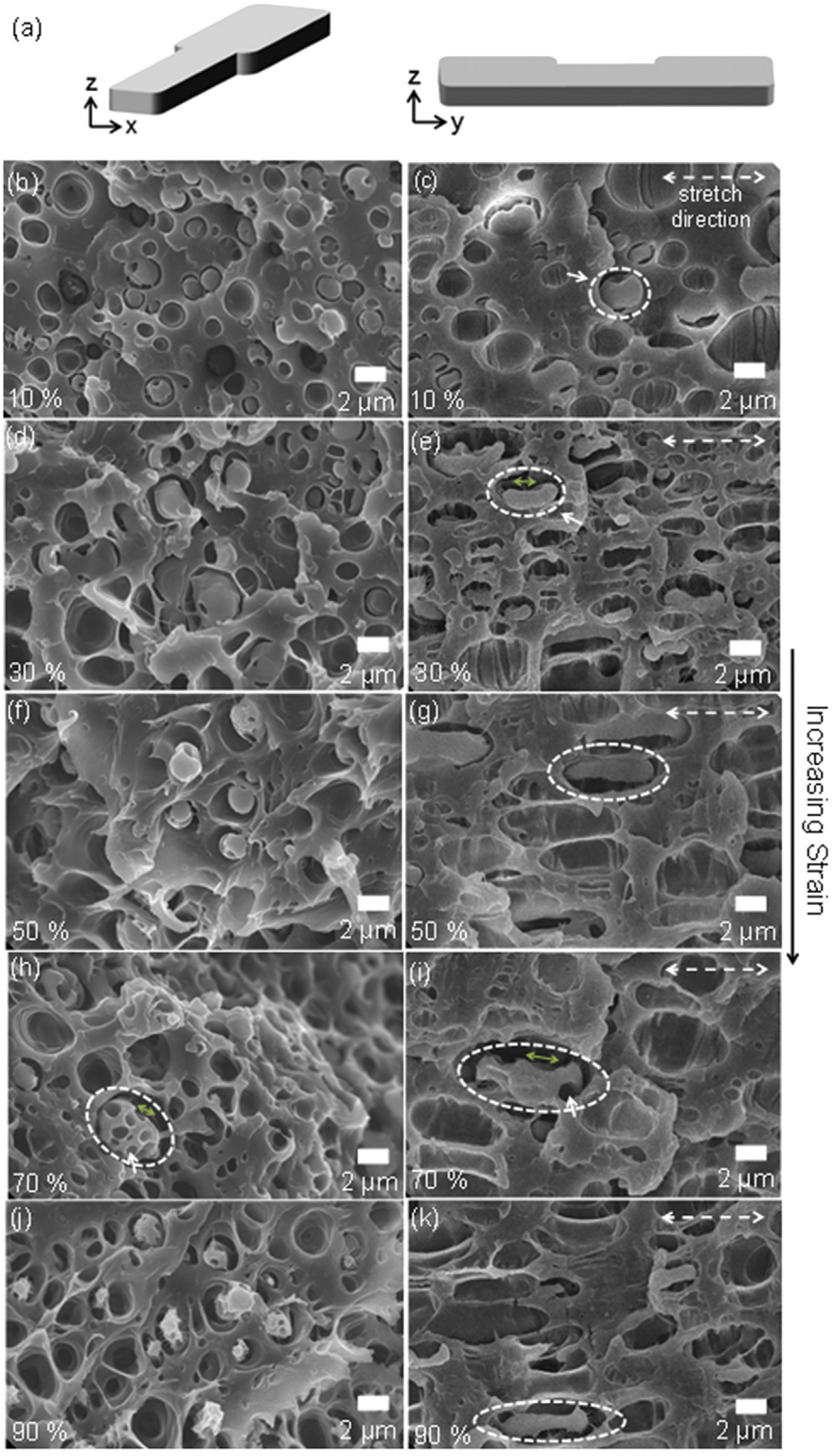

Fig. 4. SEM micrographs of cryo-fractured tensile specimen of PLA/PBE/PEGMMA/PAG (90/10/1/4) blend at different strains. (a) Cartoon of different fracture and scanning directions. Left column: examination of xz plane, transverse to the axial strain (b) 10%; (d) 30%; (f) 50%; (h) 70%; (j) 90% strain. Right column: examination of yz plane, parallel to the axial strain, (c) 10%; (e) 30%; (g) 50%; (i) 70%; (k) 90% strain. Dash circles highlight some representative PBE particles; white solid arrows highlight dents/cavities on PBE surface; green double-head arrows represent gaps between PLA and PBE; white double-head dash arrows indicate the stretch direction in tensile tests. (For interpretation of the references to colour in this figure legend, the reader is referred to the web version of this article.)

4) and PLA/PP/PAG (90/10/4) control blends without the compatibilizer (Table 1 and Figs. S9–10). In these ternary blends, although the yield stress and necking stress were reduced, the elongation at break was dramatically lower than that of the corresponding four-component blend, indicating a lack of mechanical integrity over the course of uniaxial extension and the necessity of PEGMMA as a

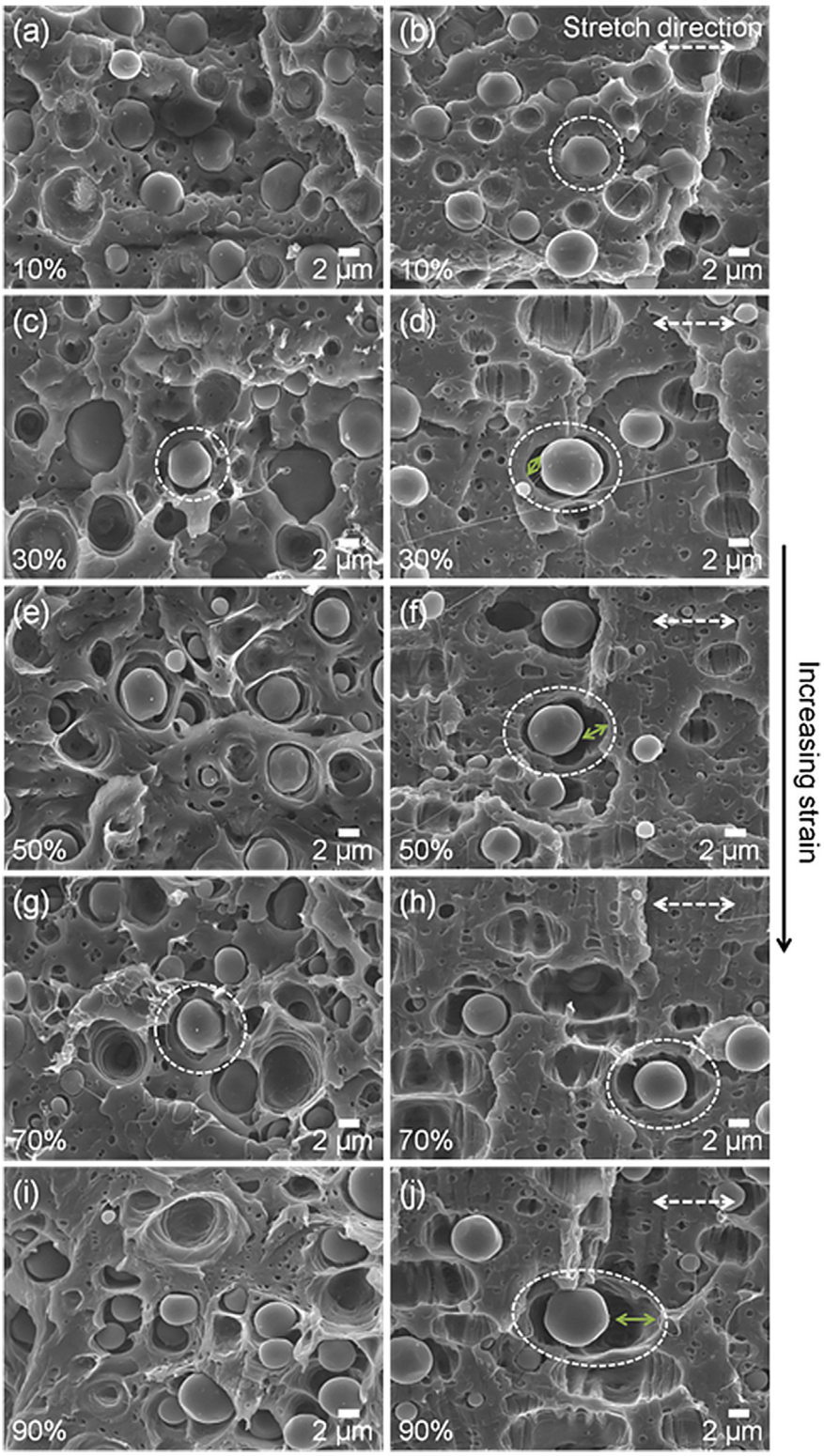

Fig. 5. SEM images of cryo-fractured tensile specimen of PLA/PP/PEGMMA/PAG (90/10/1/4) blend at different strains. Left column: examination of xz plane, transverse to the axial strain (a) 10%; (c) 30%; (e) 50%; (g) 70%; (i) 90% strain. Right column: examination of yz plane, parallel to the axial strain (b) 10%; (d) 30%; (f) 50%; (h) 70%; (j) 90% strain. Dash circles highlight some representative PP particles; green double-head arrows represent gaps between PLA and PP; white double-head dash arrows indicate the stretch direction in tensile tests. (For interpretation of the references to colour in this figure legend, the reader is referred to the web version of this article.)

reactive compatibilizer and adhesion promoter between PLA and polyolefin phases.

To further elucidate the critical role of PAG, different PAG concentrations (1–4 wt%) were blended with a PLA/PBE/PEGMMA (90/10/1) ternary blend and the resulting properties of corresponding quaternary blends were examined. The mechanical properties of these series of blends (Table S3) further support the role of PAG in blends. When 1 wt% of PAG was incorporated, it leads to a material

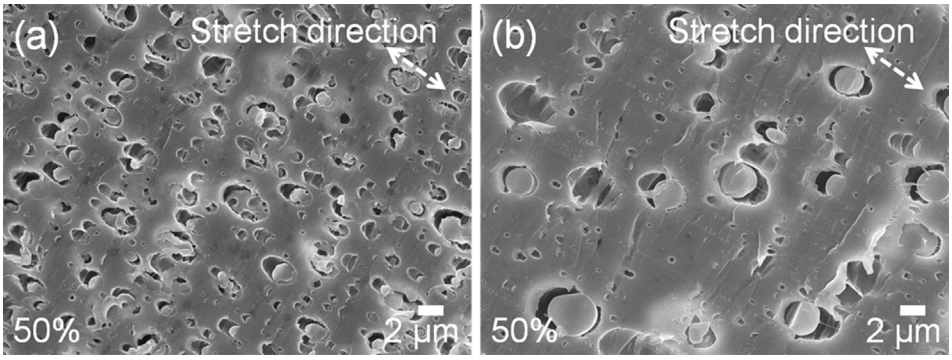

Fig. 6. Representative cryo-microtomed SEM images of blends fractured parallel to the axial strain: (a) PLA/PBE/PEGMMA/PAG (90/10/1/4) at 50% strain; (b) PLA/PP/PEGMMA/PAG (90/10/1/4) at 50% strain.

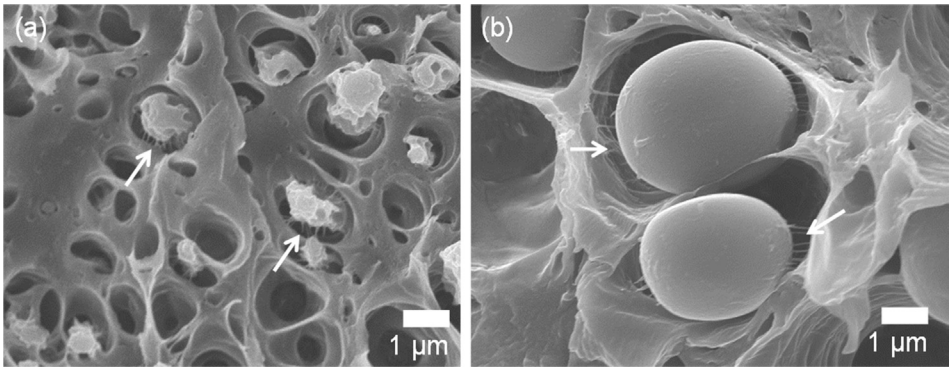

Fig. 7. Nano-fibril structures from SEM images of cryo-fractured tensile specimen at 90% strain and high magnifications. Samples fractured transverse to the axial strain. (a) PLA/PBE/PEGMMA/PAG (90/10/1/4); (b) PLA/PP/PEGMMA/PAG (90/10/1/4).

with a lower ε_b than those with higher PAG contents. Moreover, the added 1 wt% of PAG in the blend was not sufficient to improve the ε_b over its precursor blend (PLA/PBE/PEGMMA, 90/10/1). Therefore, as significant micro-voiding occurred with a PAG concentration >2 wt %, it resulted in enhanced plasticizing and interfacial modifying effects with increased ε_b and reduced yield stress (σ_{YS}). It appears that 2 wt% PAG is sufficient to produce a tough and ductile blend.

2.5. Cellular structure formation

As gleaned from the experimental results, the micro-cellular formation did not depend on the dispersed phase tested (PBE or PP), although the deformation mechanism did. The PBE droplets underwent significant deformation upon being cold drawn, in which case both dents on droplet surface and inclusion debonding mechanism led to the micro-cellular structure upon cold drawing. In contrast, for PP, the droplets showed low levels of deformation but an increased debonding effect. In both cases, besides the substantial debonding mechanism, nanoscale cavities from the cavitation of PLA matrix are also implicated in the overall micro-cellular structure. PEGMMA was used as a reactive compatibilizing agent between PLA and polyolefin phases. The nano-scale fibril linkages at the interface facilitate the stability of cellular structure during and after uniaxial extension. In addition, a low molar mass polyalkylene-glycol (PAG) served as a plasticizer and interfacial modifier, which lowered the glass transition temperature of the PLA component and yield stress of the multi-component blend as compared to the neat PLA and the PLA/polyolefin binary blend.

The micro-voiding phenomenon is also illustrated in the cartoon presented in Fig. 8. At the beginning of the uniaxial deformation, the dispersed phase (PBE or PP) acts as a stress concentrator, developing triaxial stresses in and around the uniformly dispersed droplets resulting in dilating effects at the interface near the glassy PLA matrix. Then, the debonding process is initiated and micro-voids start forming as the strain develops (depressions on the droplet surface also occur when PBE is used) [47]. These micro-voids elongate and expand along the stretching direction to dissipate the mechanical energy, and thus, form a ductile material with a cellular structure. The substantial number of micro-voids formed scatter incident light, which explains the whitening along the gauge of specimen (Fig. 3) [48].

2.6. Theoretical predictions of multicomponent blend ductile yielding

We have attributed the dramatic reduction in yield stress observed in the multicomponent blends to interfacial debonding and subsequent micro-void formation. According to the SEM images in Figs. 4 and 5, the PBE and PP inclusions debond from the PLA matrix at strains as low as 10%. We posit that the detachment of the dispersed phase takes place close to the onset of non-linearity or, in terms of stress-strain dependence, at the yield point. The effects of rigid inclusion debonding on yield and fracture stress reductions have been observed in filled polymer composites [49] and polymer blends [50]. Semi-empirical models have been developed to predict the effects of inclusion volume fraction and interfacial debonding on a reduction in stress bearing cross-section and resulting suppression of yield and fracture stresses [50,51]. Here we take a similar approach to rationalize the significant drop in yield stress observed in the multicomponent PLA/polyolefin blends.

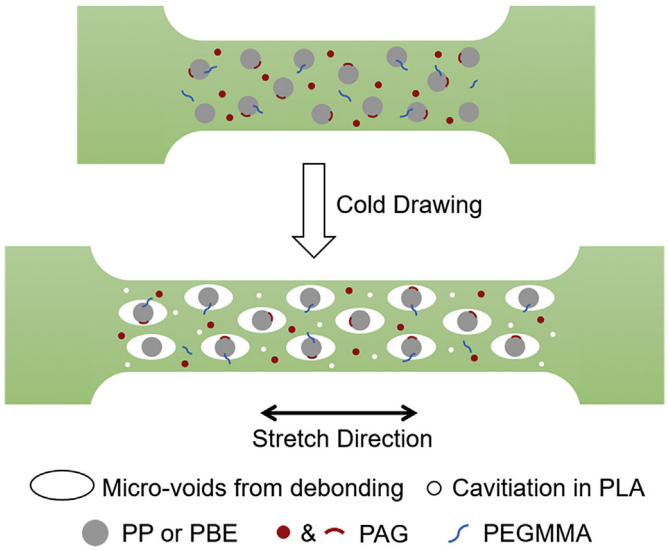

Fig. 8. Cartoon representation of the mechanical induced formation of cellular structure of PLA based multi-component blend.

For a cubic array of spherical particles that are partially detached from the PLA matrix the effective load-bearing cross-sectional area, A_{eff}, is given by

$$A_{eff} = A_o\left(1 - \beta\alpha\varphi^{2/3}\right)$$

where A_o is the initial cross-sectional area without inclusions; β is a geometrical "shape factor" with a value of 1.21 for a cubic-lattice of spherical inclusions; α is a level of debonding (0–1); and φ is the volume fraction of the inclusion. If we assume the yield stress is directly related to the effective cross-sectional area that is load bearing, the resulting yield stress ratio of a blend compared to the matrix polymer ($YSR = \sigma y/\sigma y_0$) can be expressed [50,51] as:

$$YSR = 1 - \beta\alpha\varphi^{\frac{2}{3}}$$

Compared to experimental results and accounting for differences in component densities when estimating the volume fraction of the inclusions, this semi-empirical model works well for the blends without the PAG component. The yield stress of PLA blends with PP, PBE and PEGMMA falls very close to the fully debonded inclusion prediction line (solid black) in Fig. 9a. However, the PAG containing blends fall significantly outside the fully debonded limit whether we assume the PAG forms its own inclusion phase (solid red line), or we assume complete plasticization when the yield stress of PAG-containing blend was adjusted to the yield stress of the PLA/PAG blend (dashed green). From SEM, it is apparent that PAG can form its own discrete domains. Conversely, the shifts in the T_g of PLA in the PLA/PAG blends, are indicative of PAG-plasticization of the PLA matrix; and therefore, we can reasonably expect that the yield stress of PAG containing blends should lie between these boundaries. Surprisingly, these blends demonstrate a lower effective yield stress ratio than that predicted for their inclusion volume fraction.

From the model predictions, the apparent inclusion volume content could be estimated based on the experimentally observed *YSR* values for PAG containing blends. According to Fig. 9a, the apparent volume fraction of inclusions derived from experimentally observed YSR is much larger than the inclusions true volume fraction (Fig. 9a, red curve). One plausible explanation is that yielding is occurring in the presence of debonded and non-stress-bearing inclusions (see Fig. 9b), as well as in the presence of voids having larger cross-sectional area than the inclusions (see Fig. 9b lower figure). Such an assumption is consistent with the experimental observations that during yielding, the PAG-containing blends did not neck and the cross-sectional area of drawn samples was nearly unchanged. Such deformational behavior requires volume expansion and dilational growth of micro-voids. Dilational growth of pores will decrease the effective stress-bearing cross-sectional area fraction of the blend beyond the effect of inclusions volume fraction.

According to Fig. 9a, an agreement between semi-empirical YSR predictions (red & green line) and the experimentally observed reduction in yield stress for PAG containing blends can be achieved considering the presence of micro-voids could increase the apparent volume fraction of inclusions in PAG containing blends.

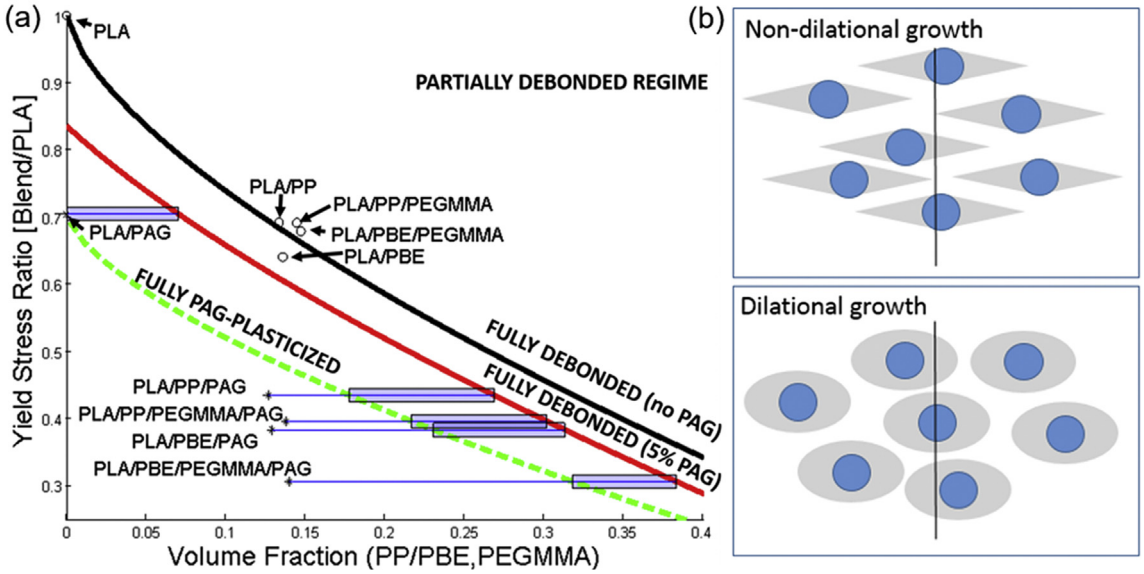

Fig. 9. (a) Yield stress ratio vs volume fraction of non-PAG components; blue rectangles represent possible ranges of apparent volume fraction of inclusions due to cavitation; (b) traditional non-dilational growth (up) vs. dilational growth (down). (For interpretation of the references to colour in this figure legend, the reader is referred to the web version of this article.)

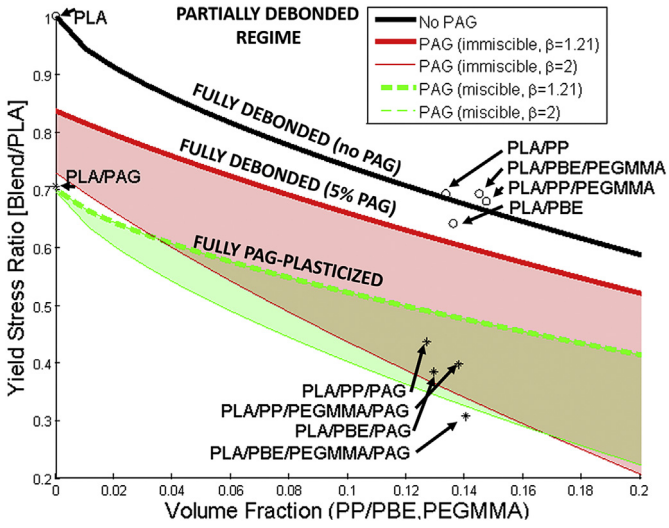

Fig. 10. Yield stress ratio vs volume fraction of non-PAG components with $\beta = [1.21, 2]$.

The effect of apparent volume fraction increase appears to be correlated with the modulus of the inclusion domain, with the softer PBE inclusions providing a larger increase. The PBE inclusions effect might be related to the differences in stress distributions around the low modulus PBE domains and more rigid PP domains, favoring dilational expansion of micro-voids around PBE inclusions.

The dilational growth of voids around inclusions could be further rationalized by adjusting the semi-empirical shape factor, β, enhancing the decrease in stress-bearing cross-sectional area. This is shown in Fig. 10 for fully immiscible PAG inclusions (red) and fully PAG plasticized regions (green), with β factor ranging between 1.21 and 2. The β factor larger than 1.21 illustrates the contribution of inclusions to void growth. The larger β factor could be a result of more voids generated during yielding. A single shape factor could not capture all PAG containing blends as the PBE inclusion trend towards a higher β factor as compared to the PP inclusions. The PEGMMA compatibilizer increases the shape factor as well, suggesting a higher volume fraction of micro-voids in PEGMMA containing blends.

2.7. Aging study

Exploring the aging phenomenon of a glassy material is a key consideration for thermoplastic materials [52–54]. In particular, PLA can show significant decreases in ductility upon aging [55]. Generally, in the case of glassy materials, the physical aging corresponds to the process where polymer chains in the glassy state relax toward equilibrium via structural relaxation processes [56]. This behavior depends on polymer structure, density and morphology. Therefore, physical aging of the PLA/PBE/PEGMMA/PAG (90/10/1/1–4) blends were analyzed by uniaxial tensile testing at different aging time (0–48 h at room temperature). The mechanical characteristics (Table S4) indicated that this multi-component material remarkably did not exhibit significant aging effect at room temperature, as the mechanical properties (ε_b, σ_{YS} and E) were very comparable within the duration of aging time (48 h).

2.8. Material density

One intrinsic advantage derived from these cellular structures of multi-component blends is the reduced density of the resulting material, which would be ideal for manufacturing lightweight polymers and reducing the cost of PLA-related products. As expected, the stretched blend at a higher strain possesses a lower material density (ρ), as presented in Fig. 11. The density of PLA/PBE/PEGMMA/PAG (90/10/1/4) before cold drawing was 1.22 g/cm^3 and dropped to 0.84 g/cm^3 at 90% strain. Similarly, the density of PLA/PP/PEGMMA/PAG (90/10/1/4) before cold drawing was 1.21 g/cm^3 and was reduced to 0.81 g/cm^3 at 90% strain, lower than that of low-density polyethylene (LDPE). In either case, the material density dropped by about 34% at 90% strain without noticeable cross-sectional area change. The percent void volume (%V_v) as determined by density measurements (described in the SI) was also used as an indication of pore volume generated within the material after being cold-drawn. At 90% strain, the percent void volume for the blend reached approximately 35% for both systems.

2.9. Mechanical properties of cold-drawn blends

Having established the cellular structure of the aforementioned PLA blends, the mechanical properties of the cold-drawn samples were evaluated. Experiments focused on subjecting the compression-molded specimen to 50% strain due to the balanced voiding and low variability during the second stage drawing. After aging for 15 min, the samples were then re-subjected to uniaxial elongation until sample failure; key results are summarized in Table S5. For voided samples from the PLA/PBE/PEGMMA/PAG (90/10/1/4) blend, the average yield stress for the cold-drawn materials (σ_{YSCD}) decreased 3-fold (to 8 MPa), and the average elongation at break of the cold-drawn (ε_{bCD}) samples was 22%. The average elastic modulus for the cold-drawn blends (E_{CD}) decreased to 0.8 GPa compared to the 1.7 GPa for the initial blends. For the PLA/PP/PEGMMA/PAG (90/10/1/4) blend, the σ_{YSCD} decreased to 10 MPa and the average ε_{bCD} was 27%. The average E_{CD} for the blend with PP as the dispersed phase also decreased to 0.9 GPa. Despite the decreases in elastic modulus and yield stress of cold-drawn blends compared to the precursors, the properties are still quite respectable.

In addition to tensile testing, the cold-drawn samples were examined under notched Charpy impact testing; processing and experimental details are provided in Supporting Information. The non-drawn blend of PLA/PBE/PEGMMA/PAG (90/10/1/4) possessed an average notched Charpy impact of 7.9 kJ/m^2 as compared to the neat PLA (3.8 kJ/m^2). After the blend was drawn to 60% at room

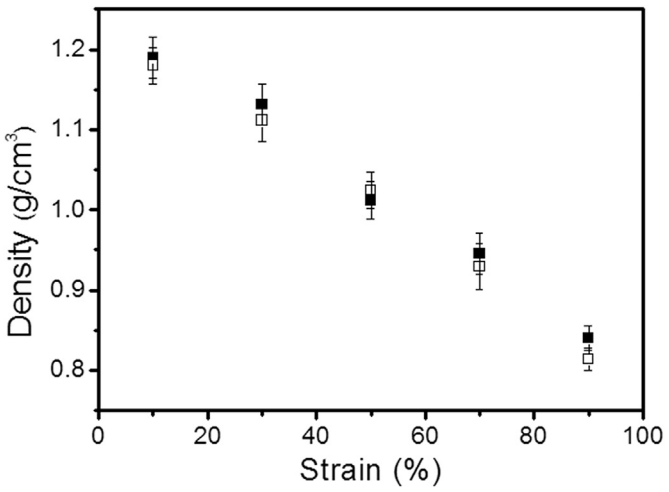

Fig. 11. Material density as a function of strain of PLA/PBE/PEGMMA/PAG (90/10/1/4), solid square; PLA/PP/PEGMMA/PAG (90/10/1/4), hollow square.

temperature, the voided material displayed an average notched Charpy impact of 53.7 kJ/m^2, 14-fold higher than neat PLA. Increases in notched Izod impact strength have been observed in PLA foams produced using supercritical CO_2 as a foaming agent [57]. However, the reported increase in notched impact was 4-fold, which is significantly lower than the results of this work. The increase in impact resistance is thought to originate from the ability of the cell walls to absorb energy during deformation, as well as stress fields initiated by micro-voids possessing sizes smaller than a critical flaw size. Overall, the novel micro-cellular blends herein have demonstrated the mechanical robustness and exceptional impact performance at a significantly lower density, as compared to the original non-voided blends.

3. Conclusions

A new family of lightweight low-density micro-cellular materials from PLA/polyolefin multi-component blends is reported. Cold drawing of the blend precursors resulted in polymeric materials with a micro-cellular structure and closed pores. The role of each individual component within the blends was evaluated, and the micro-void initiation and growth mechanism were correlated with the function of each component. Remarkably, these novel micro-cellular blend materials upon uniaxial extension showed negligible necking and a dilational expansion displaying a void volume of up to 35% and density as low as 0.81 g/cm^3 at a strain of 90%, lower than that of commercial low-density polyethylene (LDPE). SEM analysis and nitrogen sorption measurements (Fig. S11) indicated that micro-cellular materials were obtained at 30% strain for the PLA/PBE/PEGMMA/PAG and PLA/PP/PEGMMA/PAG blends. The observed reduction in yield stress of multicomponent PLA blends as compared to binary blends and several potential contributing factors were rationalized with modeling. The significant drop in blend yield stress could be attributed to inclusion debonding, PLA plasticization, and the three-dimensional expansion of micro-voids related to the inclusion domains in PAG blends. The low modulus PBE inclusions appeared to increase the contribution of micro-void expansion, further decreasing the effective load-bearing cross-sectional area and resulting in a further reduction of material yield stress.

The novel micro-cellular PLA based multicomponent blends have shown extremely high impact resistance, 14-fold higher than PLA, which is not typical for micro-cellular composites [58]. The fundamental understanding of the multi-component blends developed herein will facilitate a rational design of a new generation of low-density micro-cellular materials. Moreover, the major phase of these low-density materials was comprised of renewable and biodegradable polylactide (PLA). Ultimately, this work offers a novel and economical approach to generate micro-cellular polylactide based materials, which could have a potentially substantial impact on the applications of lightweight renewable polymers.

Acknowledgement

The authors would like to acknowledge the Kimberly-Clark Corporation for funding support, providing polymer blends, and assistance in the notched Charpy impact tests and modelling work. We also acknowledge the Center for Sustainable Polymers at the University of Minnesota, a National Science Foundation supported Center for Chemical Innovation (CHE-1413862). S.A.S acknowledges the NSF GRFP for funding. Parts of this work were carried out in the Characterization Facility, University of Minnesota, a member of the NSF-funded Materials Research Facilities Network (www.mrfn.org) via the MRSEC program.

Appendix A. Supplementary data

Supplementary data related to this article can be found at http://dx.doi.org/10.1016/j.polymer.2016.08.102.

References

[1] R. Auras, L.T. Lim, S.E.M. Selke, H. Tsuji, in: R.F. Grossman, D. Nwabunma (Eds.), Polymer Enginnering and Technology, John Wiley & Sons, Inc., New Jersey, 2010, pp. 1–16.
[2] K.S. Anderson, K.M. Schreck, M.A. Hillmyer, Toughening polylactide, Polym. Rev. 48 (2008) 85–108.
[3] R. Auras, B. Harte, S. Selke, An overview of polylactides as packaging materials, Macromol. Biosci. 4 (2004) 835–864.
[4] N. Kawahima, S. Ogawa, S. Obuchi, M. Matsuo, T. Yagi, in: first ed., in: Y. Doi, A. Steinbüchel (Eds.), Biopolymers. Polyesters III. Applications and Commercial Products, vol. 4, Wiley-VCH Verlag GmbH, Weinheim (, 2002.
[5] B. Eling, S. Gogolewski, A.J. Pennings, Biodegradable materials of poly(L-lactic acid). 1. Melt-spun and solution-spun fibres, Polymer 23 (1982) 1587–1593.
[6] H. Tsuji, R. Smith, W. Bonfield, Y. Ikada, Porous biodegradable polyesters. I. Preparation of porous poly(L-lactide) films by extraction of poly(ethylene oxide) from their blends, J. Appl. Polym. Sci. 75 (2000) 629–637.
[7] L. Fambri, A. Pegoretti, R. Fenner, S.D. Incardona, C. Migliaresi, Biodegradable fibres of poly(L-lactic acid) produced by melt spinning, Polymer 38 (1997) 79–85.
[8] A.J. Peacock, Handbook of Polyethylene: Structure, Properties, and Applications, Marcel Dekker, Inc, New York, 2000.
[9] O. Martin, L. Avérous, Poly(lactic acid): plasticization and properties of biodegradable multiphase systems, Polymer 42 (2001) 6209–6219.
[10] G.M. Gladysz, K.K. Chawla, Voids in Materials: from Unavoidable Defects to Designated Cellular Materials, Elsevier, The Netherlands, 2015, pp. 60–61.
[11] R.T. Chen, C.K. Saw, M.G. Jamieson, T.R. Aversa, R.W. Callahan, Structural characterization of Celgard® microporous membrane precursors: melt-extruded polyethylene films, J. Appl. Polym. Sci. 53 (1994) 471–483.
[12] J. Kim, S.S. Kim, M. Park, M. Jang, Effects of precursor properties on the preparation of polyethylene hollow fiber membranes by stretching, J. Membr. Sci. 318 (2008) 201–209.
[13] S.H. Tabatabaei, P.J. Carreau, A. Ajji, Microporous membranes obtained from polypropylene blend films by stretching, J. Membr. Sci. 325 (2008) 772–782.
[14] F. Sadeghi, A. Ajji, P.J. Carreau, Analysis of microporous membranes obtained from polypropylene films by stretching, J. Membr. Sci. 292 (2007) 62–71.
[15] D. Zhang, K. Kou, P. Gao, Y. Zhang, Z. Zheng, Effects of uniaxial drawing on the performance and structure of filled polytetrafluoroethylene, Polym. Eng. Sci. 54 (2014) 1427–1435.
[16] J. Wang, Z. Xu, Y. Xu, Preparation of poly(4-methyl-1-pentene) asymmetric or microporous hollow-fiber membranes by melt-spun and cold-stretch method, J. Appl. Polym. Sci. 100 (2006) 2131–2141.
[17] S. Pilla, A. Kramschuster, L. Yang, J. Lee, S. Gong, L. Turng, Microcellular injection-molding of polylactide with chain-extender, Mater. Sci. Eng. C 29 (2009) 1258–1265.
[18] M. Nofar, C.B. Park, Poly(lactic acid) foaming, Prog. Polym. Sci. 39 (2014) 1721–1741.
[19] A. Ameli, D. Jahani, M. Nofar, P.U. Jung, C.B. Park, Development of high void fraction polylactide composite foams using injection molding: mechanical and thermal insulation properties, Compos. Sci. Technol. 90 (2014) 88–95.
[20] Y. Ema, M. Ikeya, M. Okamoto, Foam processing and cellular structure of polylactide-based nanocomposites, Polymer 47 (2006) 5350–5359.
[21] A. Pawlak, A. Galeski, Cavitation during tensile deformation of polypropylene, Macromolecules 41 (2008) 2839–2851.
[22] M.F. Butler, A.M. Donald, A.J. Ryan, Time resolved simultaneous small- and wide-angle X-ray scattering during polyethylene deformation – II. Cold drawing of linear polyethylene, Polymer 39 (1998) 39–52.
[23] A. Pawlek, A. Galeski, A. Rozanski, Cavitation during deformation of semicrystalline polymers, Prog. Polym. Sci. 39 (2014) 921–958.
[24] F. Addiego, J. Di Martino, D. Ruch, A. Dahoun, O. Godard, P. Lipnik, J.J. Biebuyck, Cavitation in unfilled and nano-$CaCO_3$ filled HDPE subjected to tensile test: revelation, localization, and quantification, Polym. Eng. Sci. 50 (2010) 278–289.
[25] N.T. Scholl, R.J. McEneany, T.A. Eby, V. Topolkaraev, (Kimberly-Clark Co.) Renewable polyester compositions having a low density. US 9040598 B2 (granted May, 2015).
[26] R.J. McEneany, V. Topolkaraev, N.T. Scholl, T.A. Eby, (Kimberly-Clark Co.) Renewable polyester fibers having a low density. US 20130210308 A1 (published August, 2013).
[27] Y. Xu, J. Loi, P. Delgado, V. Topolkaraev, R.J. McEneany, C.W. Macosko, M.A. Hillmyer, Reactive compatibilization of polylactide/polypropylene blends, Ind. Chem. Eng. Res. 54 (2015) 6108–6114.
[28] A. Pawlek, A. Galeski, Cavitation during tensile drawing of semicrystalline polymers, Polimery 56 (2011) 627–636.
[29] U. Sundararaj, C.W. Macosko, Drop breakup and coalescence in polymer blends: the effects of concentration and compatibilization, Macromolecules 28 (1995) 2647–2657.
[30] S. Lyu, T.D. Jones, F.S. Bates, C.W. Macosko, Role of block copolymers on

suppression of droplet coalescence, Macromolecules 35 (2002) 7845–7855.
[31] C. Zhang, Y. Bai, Y. Sun, J. Gu, Y. Xu, Preparation of hydrophilic HDPE porous membranes via thermally induced phase separation by blending of amphiphilic PE-*b*-PEG copolymer, J. Membr. Sci. 365 (2010) 216–224.
[32] X. Li, K. Wang, Q. Fu, Thermal annealing-induced superior toughness in polypropylene/poly(ethylene glycol) blend and its structural origin, Polym. Eng. Sci. 53 (2013) 2053–2060.
[33] B.S. Park, J.C. Song, D.H. Park, K.B. Yoon, PLA/chain-extended PEG blends with improved ductility, J. Appl. Polym. Sci. 123 (2012) 2360–2367.
[34] K. Sungsanit, N. Kao, S.N. Bhattacharya, Properties of linear poly(lactic acid)/polyethylene glycol blends, Polym. Eng. Sci. 52 (2012) 108–116.
[35] Z. Kulinski, E. Piorkowska, K. Gadzinowska, M. Stasiak, Plasticization of poly(L-lactide) with poly(propylene glycol), Biomacromolecules 7 (2006) 2128–2135.
[36] T. Ke, X. Sun, Thermal and mechanical properties of poly(lactic acid) and starch blends with various plasticizers, Trans. ASAE 44 (2001) 945–953.
[37] S. Cheng, S.Q. Wang, Elastic yielding after cold drawing of ductile polymer glasses, Macromolecules 47 (2014) 3661–3671.
[38] H.H. Chuah, Orientation and structure development in poly(trimethylene terephthalate) tensile drawing, Macromolecules 34 (2001) 6985–6993.
[39] Y. Li, H. Shimizu, Toughening of polylactide by melt blending with a biodegradable poly(ether)urethane elastomer, Macromol. Biosci. 7 (2007) 921–928.
[40] K.S. Anderson, S.H. Lim, M.A. Hillmyer, Toughening of polylactide by melt blending with linear low-density polyethylene, J. Appl. Polym. Sci. 89 (2003) 3757–3768.
[41] N. Ljungberg, B. Wesslen, The effects of plasticizers on the dynamic mechanical and thermal properties of poly(lactic acid), J. Appl. Polym. Sci. 86 (2002) 1227–1234.
[42] L.V. Labrecque, R.A. Kumar, V. Dave, R.A. Gross, S.P. Mecarthy, Citrate esters as plasticizers for poly(lactic acid), J. Appl. Polym. Sci. 66 (1997) 1507–1513.
[43] L.L. Zhang, C.C. Xiong, X.M. Deng, Miscibility, crystallization and morphology of poly(β-hydroxybutyrate)/poly(*d*,*l*-lactide) blends, Polymer 37 (1996) 235–241.
[44] V. Topolkaraev, N.T. Scholl, R.J. McEneany, T.A. Eby, (Kimberly-Clark Co.) Rigid renewable polyester compositions having a high impact strength and tensile elongation. US 8975305 B2 (grated March, 2015).
[45] T. Li, V.A. Topolkaraev, A. Hiltner, E. Baer, X.Z. Ji, R.P. Quirk, Block copolymers as compatibilizers for blends of linear low density polyethylene and polystyrene, J. Polym. Sci. Part B Polym. Phys. 33 (1995) 667–683.
[46] K.S. Anderson, M.A. Hillmyer, The influence of block copolymer microstructure on the toughness of compatibilized polylactide/polyethylene blends, Polymer 45 (2004) 8809–8823.
[47] X. Sun, H. Kharbas, J. Peng, L.S. Turng, A novel method of producing lightweight microcellular injection molded parts with improved ductility and toughness, Polymer 56 (2015) 102–110.
[48] I.A. Van Casteren, R.A.M. Van Trier, J.G.P. Goossens, H.E.H. Meijer, P.J. Lemstra, The influence of hydrogen bonding on the preparation and mechanical properties of PS-diblock copolymer blends, J. Polym. Sci. Part B Polym. Phys. 42 (2004) 2137–2160.
[49] L.E. Nielsen, R.R. Landel, Mechanical Properties of Polymers and Composites, second ed., Marcel Dekker, Inc., New York, 1994.
[50] T. Li, V.A. Topolkaraev, A. Hiltner, E. Baer, Failure mechanisms in blends of linear low- density polyethylene and polystyrene, in: C.K. Riew, A.J. Kinloch (Eds.), Toughened Plastics II, Advances in Chemistry, vol. 252, ACS, 1996, pp. 319–334.
[51] S. Bazhenov, Chapter of "metal, ceramic and polymeric composites for various uses, in: J. Cuppoletti (Ed.), Mechanical Behavior of Filled Thermoplastic Polymers, InTech, 2011.
[52] P. Pan, B. Zhu, Y. Inoue, Enthalpy relaxation and embrittlement of poly(l-lactide) during physical aging, Macromolecules 40 (2007) 9664–9671.
[53] M. Kwon, S.C. Lee, Y.G. Jeong, Influences of physical aging on enthalpy relaxation behavior, gas permeability, and dynamic mechanical property of polylactide films with various D-isomer contents, Macromol. Res. 18 (2010) 346–351.
[54] C. Sheng, T. Zhang, Y. Yuan, L. Zhou, Y. Duan, J. Zhang, Effect of a small amount of poly(3-hydroxybutyrate) on the crystallization behavior of poly(L-lactic acid) in their immiscible and miscible blends during physical aging, Polym. Int. 63 (2014) 1270–1277.
[55] H. Cai, V. Dave, R.A. Gross, S.P. McCarthy, Effects of physical aging, crystallinity, and orientation on the enzymatic degradation of poly(lactic acid), J. Polym. Sci. Part B Polym. Phys. 34 (1996) 2701–2708.
[56] E.A. McGonigle, J.M.G. Cowie, V. Arrigui, R.A. Pethrick, Enthalpy relaxation and free volume changes in aged styrene copolymers containing a hydrogen bonding co-monomer, J. Mat. Sci. 40 (2005) 1869–1881.
[57] L.M. Matuana, Solid state microcellular foamed poly(lactic acid): morphology and property characterization, Bioresour. Technol. 99 (2008) 3643–3650.
[58] R.M. Christensen, Mechanics of cellular and other low-density materials, Int. J. Solids. Struct. 37 (2000) 93–104.